ISSN 1822-427X/eISSN 1822-4288
2024 Volume 19 Issue 3: 43–68
https://doi.org/10.7250/bjrbe.2024-19.642

THE BALTIC JOURNAL
OF ROAD
AND BRIDGE
ENGINEERING
2024/19(3)

INVESTIGATION OF THE NATURAL FREQUENCY CHANGE OF THE SUSPENSION BRIDGE UNDER OPERATING CONDITIONS

YAZHOU QIN[1,2*], YANSONG CUI[1]

[1]*School of Transportation and Civil Engineering, Nantong University, Nantong, China*

[2]*College of Engineering, Mathematics and Physical Sciences, University of Exeter, Exeter, UK*

Received 11 March 2024; accepted 12 August 2024

Abstract. This study addresses the challenge of accurately correlating the bridge natural frequency with influencing factors during ambient vibration by analysing on-site monitored data. This knowledge gap arises from the combined uncertainties of environmental factors and monitoring equipment noise. To tackle this challenge, the Fourier synchrosqueezed transform technique is employed and validated first by the simulated signal, as well as the Welch method. Then the instantaneous frequency of recorded acceleration at the real bridge is tracked, and a distinct diurnal pattern in the natural frequency is revealed. Then the two-stage strategy is adopted for the regression analysis. Firstly, the regression models between the normalised vibration intensity and the normalised frequency change of the vertical mode are established. Building upon these results, the additional factor, namely the effective wind speed, is considered in the second stage. The multiple linear regression model is established between the natural frequency change, the vibration intensity, and the effective wind speed. A thorough comparison of the results from both regression models reveals in-depth statistical insights. This study confirms

* Corresponding author. E-mail: yazhouqin@ntu.edu.cn

Yazhou QIN (ORCID ID 0000-0001-6190-6867)

that vibration intensity has a negative effect on the bridge natural frequency, i.e., higher vibration intensity leads to a decrease in natural frequency. Besides, the study also shows that while the effective wind speed has a statistically significant impact on the frequency change of the vertical modes, vibration intensity (caused by traffic loads) appears to be a more dominant factor.

Keywords: effective wind speed, Fourier synchrosqueezed transform, inverse relationship, instantaneous frequency, monitored vertical acceleration, Welch method.

Introduction

The utilisation of structural health monitoring (SHM) systems and modal analysis have become pervasive across various structures, serving to monitor their behaviour and detect potential malfunctions at early stages over the past few decades (Freimanis & Paeglitis, 2020; Freimanis & Paeglītis, 2019; Gatti, 2019; He et al., 2022; Ko & Ni, 2005; Koo et al., 2013; Ye et al., 2023). Among the techniques employed, operational modal analysis (OMA) stands out as particularly potent for large-scale bridges in active service. By harnessing data collected through SHM sensors, OMA facilitates continuous analysis of structural behaviour without necessitating full-scale excitation through artificial means. This avoids the need to close traffic, saving time and resources while still providing valuable insights into bridge health. However, in this case, environmental and operational loadings such as wind, temperature, traffic loading, etc. inevitably introduce uncertainty to the system identification of the bridge (Omenzetter et al., 2013; Tran et al., 2020), making it challenging to accurately identify the modal parameters of the bridge. Some effective algorithms are introduced for the OMA of bridges, such as stochastic subspace identification (SSI), the eigensystem realisation algorithm (ERA), etc. (Anastasopoulos et al., 2021; Au et al., 2021; Dederichs & Øiseth, 2023; Zahid et al., 2020). Additionally, cutting-edge time-frequency analysis techniques have been developed and employed to track the instantaneous frequency of the structures in recent years (Kareem & Kijewski, 2002; Neild et al., 2003; Silik et al., 2021). These techniques can effectively squeeze the energy of the signal around the estimated instantaneous frequency so that the resolution is improved in the frequency domain compared to the traditional methods (Gundewar & Kane, 2022; Lu & Ren, 2023; Qin, 2023; Zhang et al., 2022). Tang et al. (2023) proposed a local maximum synchrosqueezing method combined with an adaptive windowing technique to identify the instantaneous frequency of the time-dependent structures. The results show that the novel method performs better compared to other methods. Yang et al. (2024) used the Hilbert transform technique to establish a

relationship between the two contact responses of the test vehicle, then derived a simple formula for the modal damping ratio of the bridge, and its reliability was verified by a numerical model. Four time-frequency analysis techniques are employed to deal with the field measurements from the Boyne viaduct, Ireland, and the results show that wavelet synchrosqueezed transform is the best method to localize and separate the closely spaced resonances (Mostafa et al., 2021). Due to the fact that the recorded response behaviour of the bridge is often non-stationary and nonlinear under operational conditions, the synchrosqueezed transform is more suitable than other traditional methods.

Many researchers have reported that the bridge natural frequency undergoes changes during ambient vibration, as documented in their studies (Brownjohn et al., 2010; Chen et al., 2023; Ha et al., 2020; Huang et al., 2020; Westgate et al., 2015; Xu et al., 2021; Zhou & Sun, 2019). The paper (Magalhães et al., 2012) concerns the correlation of the natural frequency with the temperature and root mean square (RMS) values of the monitored signal over two years. The multiple linear regressions were established and validated. Referring to the regression models, the effects of the vibration intensity and the temperature were minimised. The novel digital twin approach was developed to predict future vortex-induced vibrations and assess the influence of vortex-induced force parameters on a long-span suspension bridge based on wind tunnel tests and numerical simulations (Zhang et al., 2024). The prediction accuracy was confirmed by comparing the predicted results with the measured ones. Górski et al. (2020) studied the variability of the model parameters of the cable-stayed highway bridge under traffic conditions. They reported that natural frequency changes within the range of 1.7% to 5.5% were observed. A steel and wooden footbridge was thoroughly investigated through in-situ experimental testing combined with finite element modelling (Nicoletti et al., 2023). The modal parameters, such as natural frequencies, mode shapes, and damping ratios, were presented. Moreover, by comparing the results obtained from the experiment and simulation, the authors demonstrated the conservative nature of the guideline for the dynamic design of the footbridge. As for the correlation between the structural strain and the temperature, two approaches, namely multiple linear regression (MLR) and WaveNet-based deep learning regression (DL), were employed (Mariani et al., 2024). The results showed the DL method was more precise, albeit more computationally intensive. These works are valuable and lay a strong foundation for further study. Building on these research results, our study primarily focuses on the effect of vibration intensity and the wind on the bridge frequency changes. This focus is crucial because

these effects may mask the real signal components, which are the real response to the defects of the bridge structure.

This study aims to correlate the bridge natural frequency with the wind and the vibration intensity and will be applied to effectively remove these effects in future work. To this end, a cutting-edge time-frequency analysis method, namely the Fourier synchrosqueezed transform (FSST), is utilised as a powerful tool in this study for tracking the instantaneous frequency of the bridge. In addition to the FSST, the Welch method is also employed to extract the bridge frequency, serving as an alternative approach to ensure the accuracy of the results. Subsequently, the normalised correlation between the vibration intensity and the bridge frequency is established with a 95% prediction interval. Finally, multiple linear regression analysis is performed, and the bridge natural frequency correlates with the wind and the vibration intensity for the vertical modes. This study contributes to the investigation of the combination effect of the wind and the vibration intensity on the natural frequency of the suspension bridge and the provision of a prerequisite work to remove or mitigate these effects for structural damage detection. The flowchart of this study is illustrated in Figure 1.

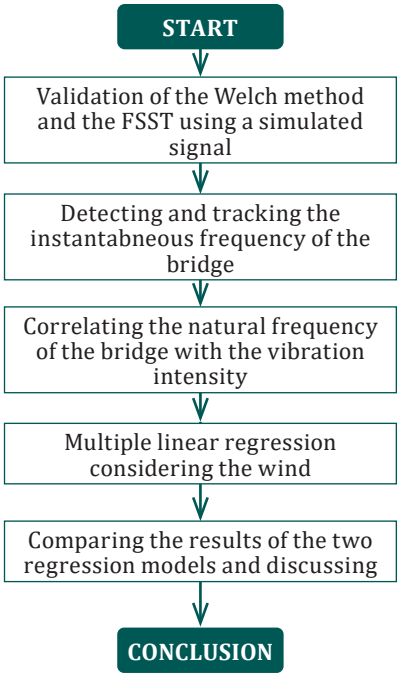

Figure 1. The flowchart of the study

This paper is structured as follows: Section 1 provides a brief review of the theory behind the Welch method and the FSST method. Section 2 utilises a simulated signal to validate the feasibility and effectiveness of the aforementioned methods. In Section 3, the Humber Bridge and its monitoring setup are introduced. Moving on to Section 4, the dynamic response data of the bridge collected at the Humber Bridge is analysed using both the Welch method and the FSST method. The diurnal trend of the bridge natural frequency is illustrated and explores the effect of vibration intensity, then the regression analysis is conducted. Subsequently, the correlation of the bridge natural frequency with the wind and the vibration intensity is established. The discussion of the results in two stages is provided in Section 5. Finally, the conclusion of this study is presented.

1. Theory of the Welch method and the FSST method

1.1. The Welch method

The Welch method is one of the classical nonparametric spectral analysis techniques that improves upon the traditional periodogram method by reducing random variations and resorting to segmenting large data samples into smaller consecutive segments. Readers can refer to (Stoica & Moses, 2005; Villwock & Pacas, 2008) for details. To implement the Welch method for a time sequence $s(n)$ with $n = 0,1,\ldots, N-1$, the primary steps are as follows (Barbe et al., 2009; Solomon Jr, 1991):

1. Partitioning and discrete Fourier transform (DFT) calculation. Partition the sequence into K segments and calculate the windowed DFT of the ith segment $s^{[i]}(n)$ at the frequency bin k;

$$s_w^{[i]}(k) = \left[\sum_{n=0}^{L-1} s^{[i]}(n)\omega\left(\frac{n}{L}\right)e^{-\frac{2\pi jkn}{L}}\right]e^{-\frac{2\pi jk}{L}\tau_i}, \tag{1}$$

where L denotes the length of a segment, $j=\sqrt{-1}$, ω is the windowing function. $\tau_i = (1-r)(i-1)/L$ represents the time delay with r being the fraction of overlap.

2. Modified periodogram formation. Form the modified periodogram values from the obtained DFT in Equation (1):

$$S_{xx}^{[i]}(k) = \left[\sum_{n=0}^{L-1}\omega\left(\frac{n}{L}\right)^2\right]^{-1}\left|s_w^{[i]}(k)\right|^2. \tag{2}$$

3. Power spectral density (PSD) estimation. Averaging the periodogram values from Equation (2) to obtain the final PSD estimate:

$$\tilde{S}_{xx}(k)=\frac{1-r}{K}\sum_{i=1}^{K/(1-r)}S_{xx}^{[i]}(k). \tag{3}$$

1.2. The FSST method

The FSST is an advanced signal processing technique that extends the capabilities of the short-time Fourier transform (STFT). By using a post-processing technique, the FSST enhances the resolution of the representation both in time domain and frequency domain obtained from the STFT, effectively squeezing the energy of individual components of the signal along the estimated instantaneous frequencies in the time-frequency plane. The significant steps involved in the FSST technique are as follows (Auger et al., 2013; Oberlin et al., 2014)

1. Calculating the STFT coefficients of the signal $s(t)$. The STFT is computed using a sliding windowing function represented by h at time t and frequency η, and it can be mathematically expressed by:

$$V_s(\eta,t)=\int_{-\infty}^{+\infty}s(\tau)h(\tau-t)e^{-2\pi i\eta(\tau-t)}\,\mathrm{d}\tau. \tag{4}$$

Here, τ is the time variable.

2. The instantaneous frequency estimation. The instantaneous frequencies of the signal are estimated by taking the derivative of each STFT coefficient with respect to t, as shown in Equation (5):

$$\tilde{\omega}_s(\eta,t)=\frac{1}{2\pi}\partial_t\arg V_s(\eta,t). \tag{5}$$

Here, $\arg V_s(\eta, t)$ represents the argument of the complex-valued STFT coefficient at time t and frequency η.

3. Reassignment of the energy around the estimated frequencies. The energy of each point in the STFT is reassigned to a new position in the time-frequency plane based on the computed instantaneous frequencies in Equation (5). This is done under the condition that the function g is continuous and does not vanish at 0, as described in Equation (6):

$$T_s(\omega,t)=\frac{1}{g(0)}\int_{-\infty}^{+\infty}V_s(\eta,t)\delta(\omega-\tilde{\omega}_s(\eta,t))\mathrm{d}\eta, \tag{6}$$

where $\delta(\ldots)$ is the Dirac distribution.

Overall, by applying the synchrosqueezed transform to the STFT, the FSST technique is capable of improving the time-frequency resolution and making the representation more interpretable.

2. Numerical validation

In this section, a simulated multi-component signal is used to validate the effectiveness of the proposed methods. The simulated signal is composed of three components, and the mathematical expression of each component of the signal is illustrated in Equation (7). The second component of the simulated signal is a piecewise function, whose modal frequency changes from 5.5 Hz to 7 Hz at a time instant of 10 s. Meanwhile, the frequency of the third component changes from 2 Hz to 3 Hz continuously. The signal has a duration of 20 s and is sampled at a frequency of 100 Hz.

$$\begin{aligned} x_1 &= 2\sin(22\pi t) \\ x_2 &= \begin{cases} 1.5\sin(11\pi t) & (0 \le t \le 10) \\ 1.5\sin(14\pi t) & (10 < t \le 20) \end{cases} \\ x_3 &= \cos(4\pi t + 0.05t^2) \\ t &\in [0, \quad 20] \end{aligned} \tag{7}$$

To account for a noise contamination scenario in practical situations, the original simulated signal is combined with Gaussian white noise. The signal-to-noise ratio (SNR) is set to 0, which means that in the heavy noise-added case, the intensity of the noise is the same as the original signal. The waveform of the simulated signal with noise is shown in Figure 2(a).

The Welch method is first employed to detect the frequency of the simulated signal. Herein, a Hanning window is applied, and the overlap fraction is set to 2/3 of the time-window length, and different lengths of the window are employed to find the best one. The obtained PSD plot is presented in Figure 2(b). It is evident from Figure 2(b) that the three constant frequencies specified in Equation (7) are accurately captured by the Welch method with a large window length. However, the time-dependent frequency of component 3 is not detected. On the one hand, Figure 2(b) highlights the advantage of the Welch method in accurately identifying stationary frequencies; on the other hand, necessary strategies should be taken to make it feasible to track the time-varying frequencies.

The FSST method is secondarily employed to directly detect the time-varying characteristics of the same simulated signal, and the

time-frequency representation of the noisy simulated signal is shown in Figure 3(a). Compared to the Welch method, changes over time in each mode of the simulated signal are distinctly tracked. Besides, the colour bars in Figure 3(a) are well consistent with the true instantaneous frequencies, which are represented by red dashed lines. Figure 3(a) appears much dirty due to the heavy added noise. The yellow colour in Figure 3(a) represents a higher energy, which indirectly reflects the amplitude of the signal components.

(a) The simulated signal with noise (from top to bottom are components 1, 2, 3, noise, and noisy signal)

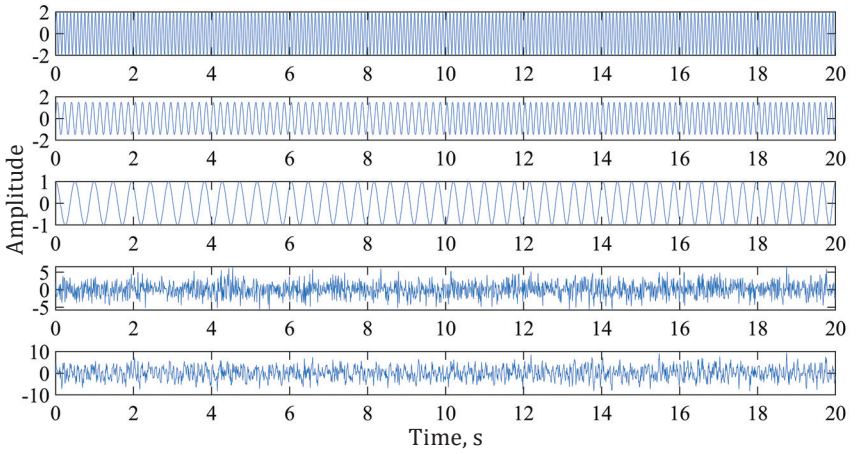

(b) The PSD plot

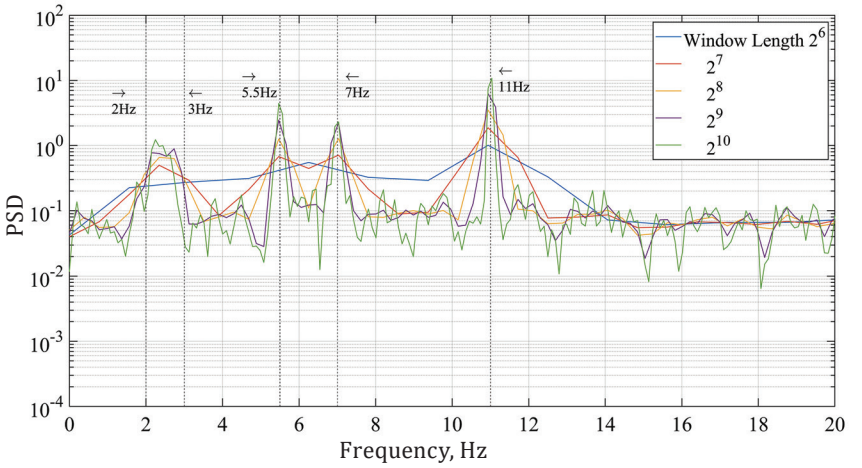

Figure 2. The waveform of the noisy simulated signal and its spectra

Figure 3(b) shows the extracted instantaneous frequencies of the noisy simulated signal obtained by using the ridge technique. It can be observed that the instantaneous frequencies of all components are detected accurately, although there is a bit of a difference in the beginning and the end due to the boundary effects in the third component. Overall, the results obtained are shown acceptable for tracking the instantaneous frequency.

(a) The time-frequency representation

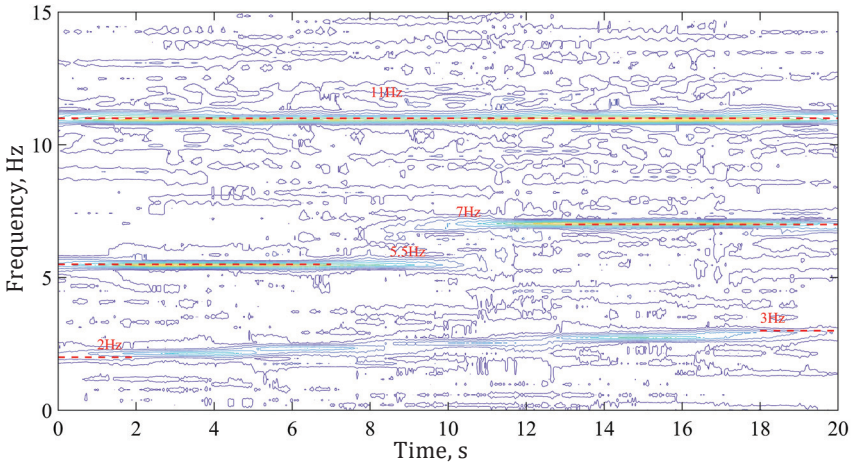

(b) The extracted instantaneous frequencies

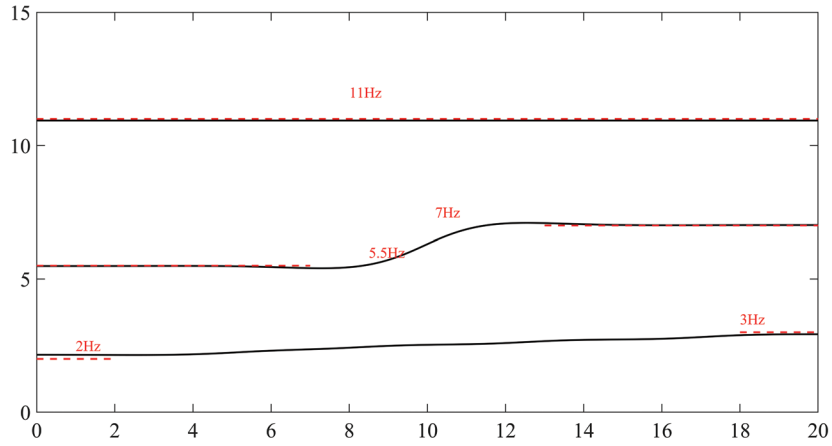

Figure 3. The time-frequency representation and instantaneous frequencies of the simulated signal (the red dashed lines are the true instantaneous frequencies in Equation (7))

3. The monitoring system at Humber Bridge

The Humber Bridge is a suspension bridge that spans the River Humber and connects Hessle in East Yorkshire with Barton in North Lincolnshire. Designed to accommodate the A15 dual carriageway, it boasts a main span of approximately 1410 m, with side spans of 280 m and 530 m, respectively. The carriageway of the Humber Bridge features a 4.5-meter-deep steel deck box, separated by two reinforced concrete towers. The two 3-meter-wide walkways on each side are comprised of panels cantilevered from the edges of the deck boxes. Figure 4 shows the location of the bridge and the layout of the monitoring system.

Three QA750 servo-accelerometers were installed in the middle of the main span of the Humber Bridge. The resolution of the QA750 is better than 1 μg, and the sensor noise floor is less than 3 $\mu g/\sqrt{Hz}$ in the range from 0 to 10 Hz. Two accelerometers are mounted at the mid-span on the east and west sides of the deck in the vertical direction, as shown in Figure 4(b), marked with red dots. They are primarily used to measure the vertical and torsional dynamic responses of the bridge. The third accelerometer is installed inside the deck box near the centre of

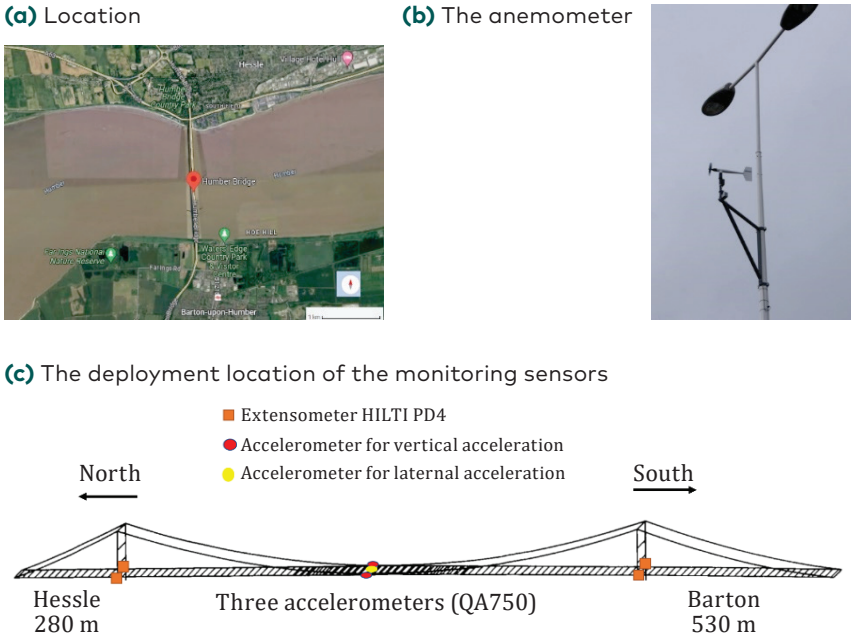

Figure 4. The location of the Humber Bridge and the layout of the monitoring system

the carriageway and oriented horizontally to provide continuous lateral acceleration records of the bridge, as shown in Figure 4(b) with a yellow dot. Along with these accelerometers, the RM Young 05305 anemometer was also installed on a lamppost, as shown in Figure 4(c) (Brownjohn et al., 2020). The key parameters of this anemometer are:

- Wind speed measurement: Range of 0 to 50 m/s (112 mph) with a threshold sensitivity: 0.4 m/s (0.9 mph);
- Wind direction measurement: Mechanical range of 360° and electrical range of 355°, with a threshold sensitivity of 0.5 m/s (1.0 mph) at 10° displacement and 0.7 m/s (1.6 mph) at 5° displacement.

The data acquisition system was set with a sampling rate of 20 Hz, and each acceleration time series recorded by the servo-accelerometers was divided into 30-minute segments. One of these segments recorded from 14:36 to 15:06 on 1 February 2012 is plotted in Figure 5(a).

4. Analysis of the monitored acceleration at the Humber Bridge

4.1. Tracking the bridge natural frequencies

By using the monitoring equipment mentioned above, three accelerations and the wind are recorded and stored during the monitoring period. The collected signal data are pre-processed first, and the detrend function is used. Given the crucial significance of low frequencies for the suspension bridge, the modal frequencies below 2 Hz are focused. The vertical acceleration at the Humber Bridge is used herein for its sensitivity to the vibration intensity induced by the traffic load. The Welch method and the FSST method are employed to deal with the 30-minute acceleration segment from 14:36 to 15:06 on 1 February 2012. The acceleration signal and the results obtained are shown in Figure 5, as well as the PSD plot for the whole day.

Figure 5(b) shows the PSD plot for the 30-minute acceleration segment from 14:36 to 15:06 on 1 February 2012. Compared to the reference frequencies in the literature (Brownjohn et al., 1987; Brownjohn et al., 2010), the difference between them is almost negligible. Figure 5(c) displays the time-frequency representation obtained by the FSST method. It can be seen that the vertical modes are clearly separated. The red dashed lines in Figure 5(c) are the instantaneous frequencies of the bridge extracted, and the fluctuations of the instantaneous frequencies over time are clearly observed.

However, it should be noted that Figure 5(c) appears slightly ambiguous due to the noise caused by environmental and operational factors. Despite this, Figure 5(c) demonstrates the FSST as a powerful tool for accurately tracking the change in the bridge frequencies of the vertical modes over time under in-service conditions. Figure 5(d) displays the PSD plot for the whole day by the Welch method. By using the Welch method, a total of 48 30-minute accelerations monitored at the Humber Bridge during the day were processed. It is worth noting that the extracted frequency values for the same mode are slightly different due to the acceleration data collected at different monitoring times. It also reflects the bridge natural frequency change over time.

Then these 48 acceleration segments were dealt with using both methods in chronological order for the day. The extracted modal frequencies of the bridge are presented in Figure 6. For simplicity, only four modes are illustrated. In Figure 6, the red lines represent modal

(a) The 30-minute vertical acceleration

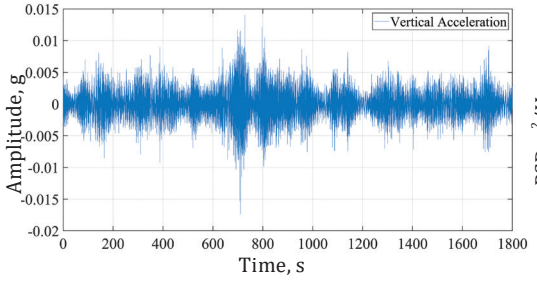

(b) PSD plot of the signal in (a) with vertical red dashed lines representing reference frequencies from literature

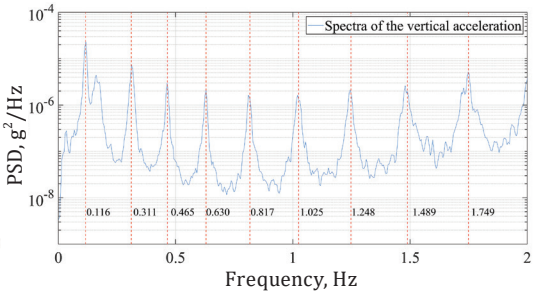

(c) Time-frequency representation of the signal in (a) with red dashed lines denoting extracted instantaneous frequencies

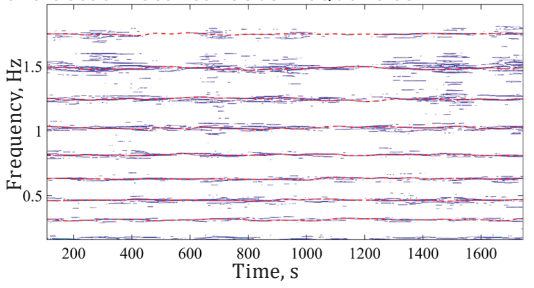

(d) The PSD plot for the entire day

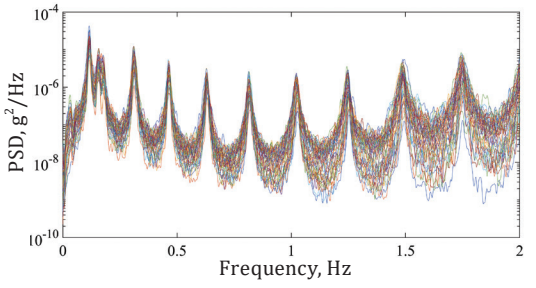

Figure 5. Monitored vertical acceleration data from 14:36 to 15:06 on 1 February 2012, with corresponding spectral plots and representation.

frequencies obtained by the Welch method, while the black dashed lines denote the instantaneous frequencies extracted by the FSST. It is noteworthy that the lowpass function is used to make the extracted instantaneous frequencies smoother. Overall, the results obtained by the two methods are in good agreement.

It can be seen in Figure 6 that the modal frequencies of the bridge are time-dependent under in-service conditions. The diurnal pattern of the bridge natural frequencies of the vertical modes is clearly observed in Figure 6. In general, the bridge natural frequencies decrease in the beginning, reach a relatively lower level, and then gradually increase over time. During the period approximately from 8:00 to 18:00, a distinguished trough appears.

4.2. Correlation between the vibration intensity and the bridge natural frequencies

It is a challenge to accurately quantify the traffic load, primarily due to the limitations of the available measuring devices. One straightforward approach involves using the moving masses on the

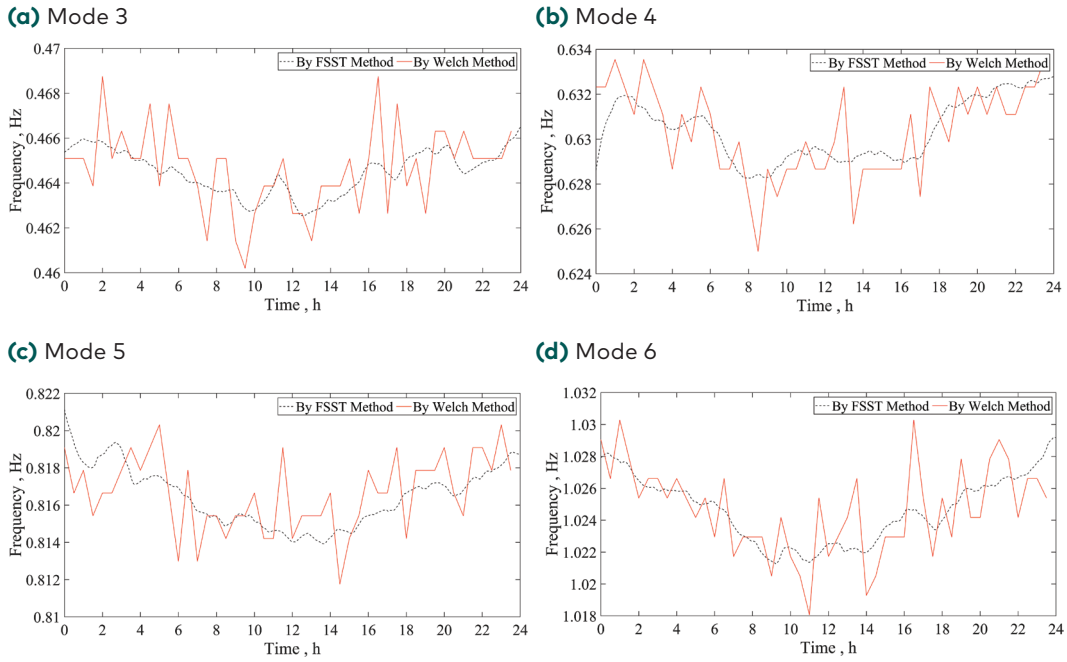

Figure 6. The extracted instantaneous frequencies by the Welch method and the FSST during the day

bridge (Cheynet et al., 2020; Prat, 2001), but it is generally too simple to reflect the real traffic load on the bridge. Other methods involve using a bridge weigh-in-motion (WIM) system if available (Lu et al., 2019; Maljaars, 2020; Zheng et al., 2022; Zhou et al., 2021). Nevertheless, the WIM system was not available at the Humber Bridge at that time. Referring to previous research studies, the root mean square (RMS) value of the bridge vertical acceleration can be used as an equivalent traffic load, which was tested with a correlation coefficient of nearly 0.7 between them (Ho & Nishio, 2020; Wattana & Nishio, 2017; Zhang et al., 2002; Zhou & Sun, 2019). Building on the aforementioned works, the RMS value of the monitored vertical acceleration, namely the vibration intensity, is used as an indirect measurement of the traffic load. The vibration intensity of the monitored vertical acceleration is plotted in Figure 7, along with the variation of the bridge instantaneous frequencies obtained by the FSST during the day. Herein, modes 3 to 6 are taken as examples shown in Figure 7.

Figure 7 overall reveals an opposite trend between the bridge natural frequency change and the vibration intensity. In other words, the relative decrease in the bridge instantaneous frequency, approximately from 8:00 to 18:00, corresponds to the higher vibration intensity during the

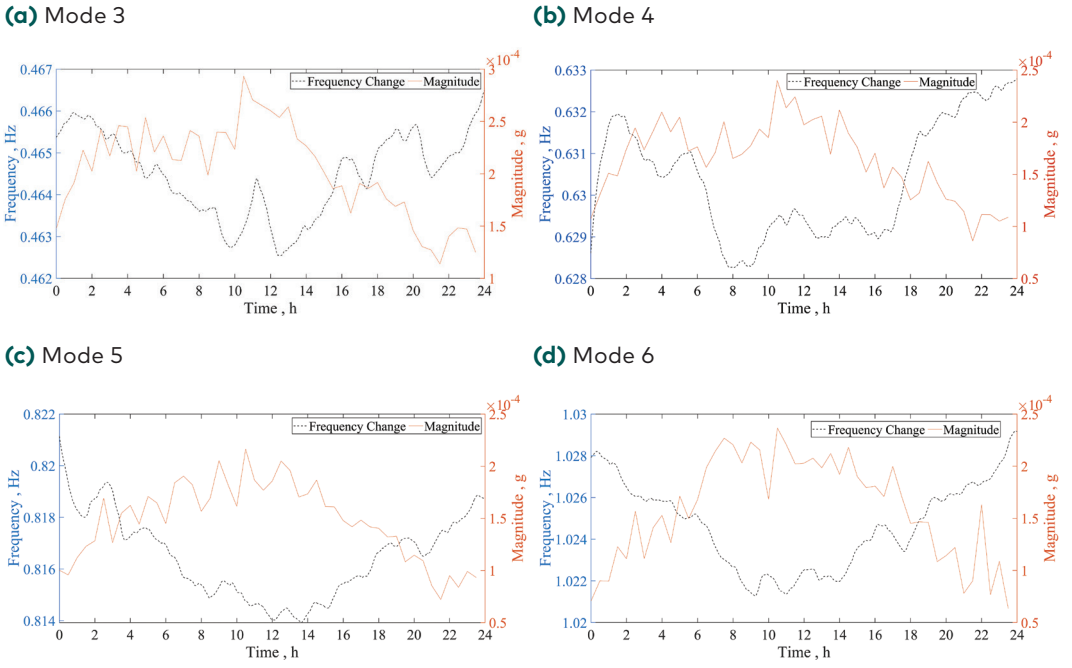

Figure 7. The vibration intensity and the bridge instantaneous frequencies

same period at the Humber Bridge. This observation implies a possible inverse relationship between the vibration intensity and the variation of the bridge natural frequency for the vertical modes. This inverse relationship aligns with the fact that the increased traffic load on the bridge acts as an additional mass for the bridge, resulting in a decrease in its natural frequency. To quantitatively establish this correlation, the linear polynomial is fitted to the monitored data along with a 95% prediction interval. The results for the four modes are shown in Figure 8. The detailed coefficients of the regression model are listed in Table 1. Notably, both the vibration intensity and the variation of the natural frequencies of the bridge are normalised before conducting the regression analysis. The normalised vectors have a mean of zero and a standard deviation of one.

Figure 8 demonstrates that the linear regression model nearly encompasses all data points, suggesting the model effectiveness is acceptable with few outliers. Moreover, the inverse relationship between the normalised vibration intensity and the normalised changes of the bridge natural frequency holds for almost all vertical modes below 2 Hz at the Humber Bridge.

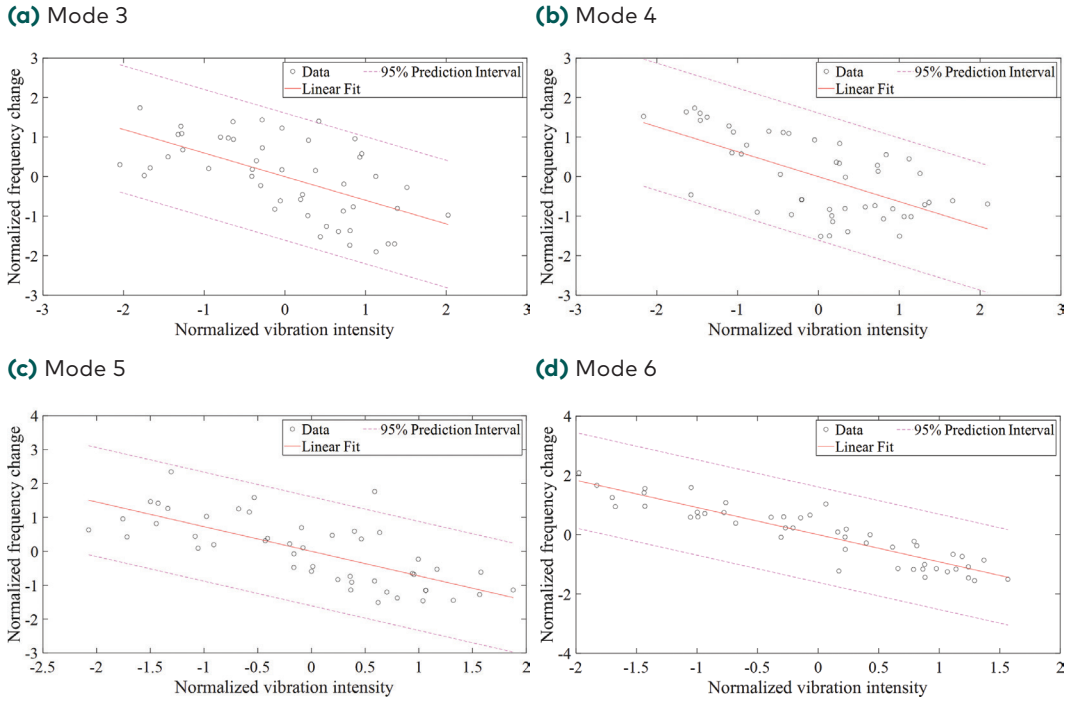

Figure 8. The correlation between the normalised vibration intensity and the normalised bridge frequency change for four modes

Table 1. Coefficients of the regression model between the normalised vibration intensity and the normalised variations of the bridge natural frequencies at the Humber Bridge

Coefficient	Mode 1	Mode 2	Mode 3	Mode 4	Mode 5	Mode 6	Mode 7	Mode 8	Mode 9
Slope parameter *a*	−0.325	−0.110	−0.597	−0.631	−0.727	−0.916	−0.804	−0.733	−0.627
R^2	0.106	0.012	0.356	0.398	0.528	0.84	0.646	0.537	0.393
p-value	0.024	0.458	0	0	0	0	0	0	0

Table 1 presents the coefficients of the regression model between the normalised vibration intensity and the normalised variations of the bridge natural frequency at the Humber Bridge. The table includes the slope parameter a, the coefficient of determination R^2, and the p-values for each mode. It can be observed in Table 1 that the p-values of all modes but mode 2 are below 0.05, which means the regression models are of statistical significance. A strong correlation exists in modes 5, 6, 7, and 8, where the coefficients R^2 are all beyond 0.5, which means the regression models can explain at least 50% of the variability in the natural frequency of the bridge. For mode 2, the coefficient of determination R^2 is near zero and the p-value exceeds 0.05, all indicating no such correlation in mode 2. Further investigation is conducted in the following subsection and discussion for this mode. Some works have reported a similar relationship between the traffic load and the bridge frequency change as presented in this study. For instance, Zhou & Sun (2019) reported negative correlations between the traffic load and the natural frequency change of the bridge at lower frequencies at Donghai Bridge. Westgate et al. (2015) reported a similar negative linear relationship between the traffic load and the natural frequency at Tamar Bridge.

4.3. Consideration of the wind effect

Based on the above-mentioned regression model between the natural frequency change of the bridge and the vibration intensity, another factor of the wind is considered in this subsection. The wind speed and wind direction are monitored by using the anemometer mounted on the lamp pole. The monitored wind speed and the wind rose on 1 February 2012 are shown in Figure 9.

Stronger wind appears between 2:30 a.m. and 5:00 a.m. and from 10:30 to 12:00, exceeding 13 m/s, as evident from Figure 9. The wind

direction was mainly from the west during this day, with smaller portions from the WSW, as Figure 9(b) shows. To account for the combined effect of the wind direction and speed, an "effective wind speed" is introduced, considering the angle between the wind direction and the normal direction (perpendicular) to the bridge longitudinal axis. This approach combines the direction and speed into a single scalar value, the effective wind speed. Figure 10 then presents the 3D scatter diagrams between natural frequency change, vibration intensity, and wind, using the effective wind speed as the wind parameter.

(a) The wind speed

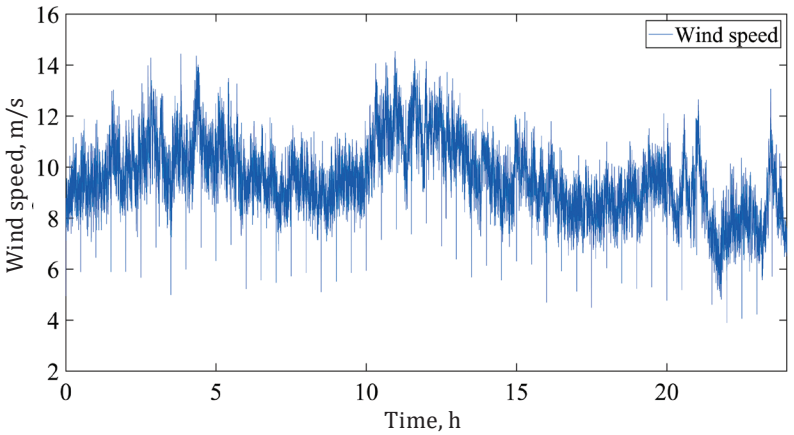

(b) The wind rose

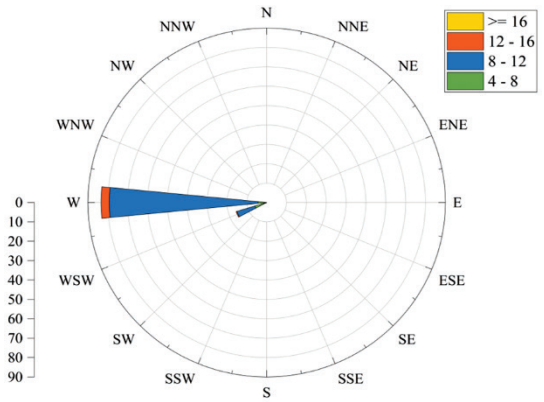

Figure 9. The monitored wind speed and wind rose diagram on 1 February 2012

In Figure 10, all data are normalised with a mean of 0 and a standard deviation of 1. The linear relationship appears clearer for mode 6, as shown in Figure 10(d). The multiple linear regression is conducted for all nine modes. Here, only two architectures of the regression model are presented as examples in Figure 11.

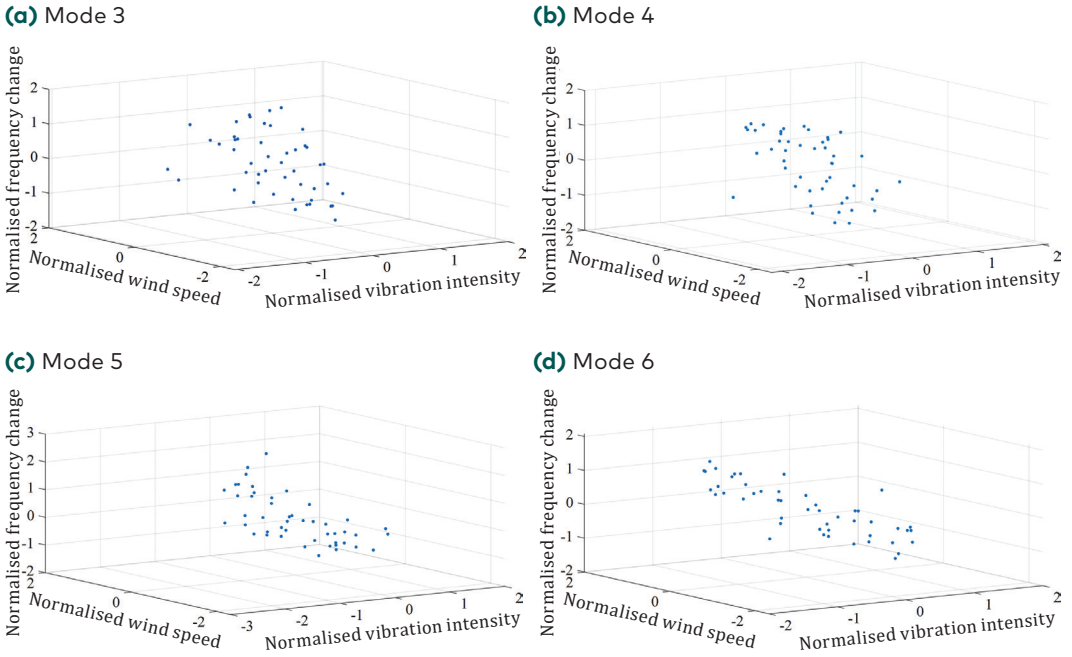

Figure 10. The 3D scatter diagrams of the normalised frequency change

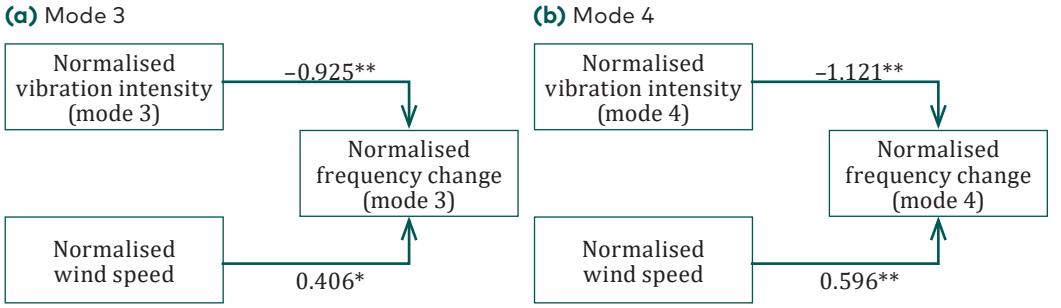

Note * represents a p-value <0.05
** represents a p-value <0.01

Figure 11. The architectures of the regression models for mode 3 and mode 4

For mode 3 in Figure 11(a), it can be observed that the coefficient of the vibration intensity is −0.925, which is statistically significant with a p-value <0.01. It indicates the vibration intensity is negative for the bridge natural frequency change. Meanwhile, the wind is also of statistical significance, with its p-value <0.05 and a value of 0.406. It implies that the increase in wind speed leads to the natural frequency growing larger. A similar explanation is for mode 4 as well. Besides, the diagrams of the coefficients with a 95% confidence interval for modes 1, 2, and 4 are presented in Figure 12 as examples.

Figure 12(a) shows the coefficients for mode 1. It can be seen that the 95% confidence interval of both coefficients includes 0, which indicates both coefficients are not statistically significant. It can also be found in the F-value and p-value of the model listed in Table 2. Figure 12(b) shows that the vibration intensity does not affect the natural frequency change because the 95% confidence interval of this coefficient includes 0, whereas the wind speed definitely has an impact on the natural frequency change for mode 2 in the statistical sense. For mode 4, both the vibration intensity and the wind speed all affect the natural frequency change in a statistical sense. Figure 13 displays the diagrams of the regression standardized residuals for mode 1 and mode 5. It can be observed that the regression standardized residual for mode 1 exhibits non-normality compared to mode 5, which indicates the poorer explanatory capability of the regression model for mode 1.

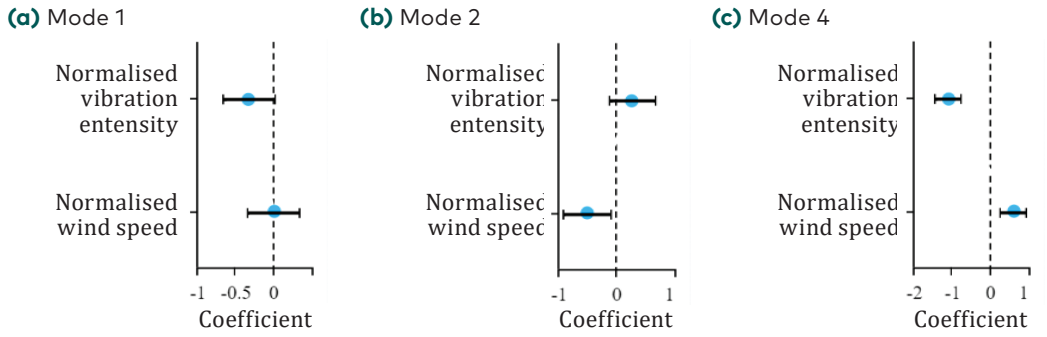

Figure 12. The diagrams of the regression coefficients with a 95% confidence interval

Table 2 lists the results obtained by using the multiple linear regression models. It can be seen that the *p*-values of the models are almost all below 0.05 except mode 1, with a *p*-value of 0.081. Besides, the coefficients of the vibration intensity are almost negative values for almost all modes except mode 2, which agrees well with the results in Table 1.

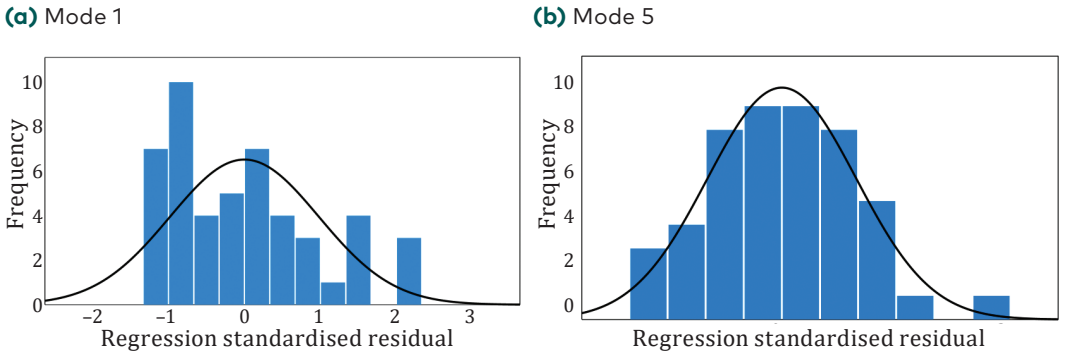

Figure 13. The diagrams of the regression standardized residuals

Table 2. Coefficients of the multiple linear regression model

		Mode 1	Mode 2	Mode 3	Mode 4	Mode 5	Mode 6	Mode 7	Mode 8	Mode 9
Slope parameter *a*	Factor 1	−0.325	0.267	−0.925	−1.121	−0.894	−0.891	−0.789	−0.741	−0.518
	Factor 2	0.001	−0.507	0.406	0.596	0.274	−0.072	−0.065	0.034	−0.371
Significance of the parameter *a*	Factor 1	0.065	0.206	<0.001	<0.001	<0.001	<0.001	<0.001	<0.001	<0.001
	Factor 2	0.995	0.019	0.042	0.002	0.031	0.257	0.477	0.746	0.001
R-square		0.105	0.127	0.414	0.513	0.575	0.844	0.65	0.539	0.519
F		2.654	3.278	15.86	23.72	30.47	121.9	41.78	26.26	24.25
p-value of the model		0.081	0.047	<0.001	<0.001	<0.001	<0.001	<0.001	<0.001	<0.001
Collinearity statistics (VIF)		1.491	2.233	2.877	3.083	1.592	1.141	1.055	1.062	1.094

Note: Factor 1 is the normalised vibration intensity, while factor 2 is the normalised wind speed. The VIF represents the variance inflation factor.

5. Discussion

Comparing the results in Table 2 to those in Table 1 reveals several key points. Adding the factor of wind speed changes, the *p*-value of the regression model for mode 1 went from below 0.05 (*p*-values less than 0.05 are typically considered statistically significant) to 0.081, indicating a loss of statistical significance. This suggests that neither vibration intensity nor wind speed has a statistically significant impact on the natural frequency change of the bridge in this mode. Double-checking the multicollinearity using the variance inflation factor (VIF) confirms no issue in this regard. However, the extracted instantaneous frequency for mode 1 exhibits some spikes, potentially implying the influence of other unknown factors.

In contrast, the *p*-value for mode 2 changes from above 0.05 to 0.047, indicating that both vibration intensity and wind speed have a statistically significant impact on the bridge natural frequency change. This highlights the importance of considering wind alongside vibration intensity for understanding the dynamics of mode 2. Notably, the slope parameters of the vibration intensity in Table 2 remain mostly negative, mirroring those in Table 1 and confirming the expected inverse relationship between vibration intensity and the bridge natural frequency.

Finally, including wind speed increases the *R*-square value of the regression model for mode 2 in Table 2. Comparing the *R*-square values across both tables along with the values of the slope parameters (parameter *a*) suggests that vibration intensity likely has a greater effect on the natural frequency change than wind speed for the vertical modes of the Humber Bridge. However, it is worth noting that the aforementioned results are obtained based on the monitored data collected at the Humber Bridge and are only valid for the natural frequency of the bridge. Moreover, the results should be further confirmed in future research.

Conclusions

The accelerometer data and wind data recorded at the Humber Bridge throughout the day were utilised to correlate the natural frequency of the bridge with environmental factors. The FSST method and Welch method were employed for this purpose. The instantaneous frequencies derived from the FSST were closely aligned with those obtained through the Welch method. The diurnal pattern of the instantaneous frequencies of the bridge was observed, consistent

with results in some literature. The linear regression results revealed that the inverse correlations between the vibration intensity and the bridge natural frequency change were generally present for almost for all modes. Furthermore, the additional factor of wind was considered simultaneously, and multiple linear regression models were proposed. The results showed that although the vibration intensity and the wind speed had a significant impact on the bridge frequency change in the vertical modes, the vibration intensity accounted for more of it.

Acknowledgements

The authors express their gratitude to Dr Ki Young Koo at the University of Exeter for providing the monitoring data and contributing to the code.

REFERENCES

Anastasopoulos, D., De Roeck, G., & Reynders, E. P. (2021). One-year operational modal analysis of a steel bridge from high-resolution macrostrain monitoring: Influence of temperature vs. retrofitting. *Mechanical Systems and Signal Processing, 161*, Article 107951. https://doi.org/10.1016/j.ymssp.2021.107951

Au, S.-K., Brownjohn, J. M., Li, B., & Raby, A. (2021). Understanding and managing identification uncertainty of close modes in operational modal analysis. *Mechanical Systems and Signal Processing, 147*, Article 107018. https://doi.org/10.1016/j.ymssp.2020.107018

Auger, F., Flandrin, P., Lin, Y.-T., McLaughlin, S., Meignen, S., Oberlin, T., & Wu, H.-T. (2013). Time-frequency reassignment and synchrosqueezing: An overview. *IEEE Signal Processing Magazine, 30*(6), 32–41. https://doi.org/10.1109/MSP.2013.2265316

Barbe, K., Pintelon, R., & Schoukens, J. (2009). Welch method revisited: nonparametric power spectrum estimation via circular overlap. *IEEE Transactions on Signal Processing, 58*(2), 553–565. https://doi.org/10.1109/TSP.2009.2031724

Brownjohn, J., Dumanoglu, A., Severn, R., & Taylor, C. (1987). Ambient vibration measurements of the Humber Suspension Bridge and comparison with calculated characteristics. *Proceedings of the Institution of Civil Engineers, 83*(3), 561–600. https://doi.org/10.1680/iicep.1987.335

Brownjohn, J. M., Magalhaes, F., Caetano, E., & Cunha, A. (2010). Ambient vibration re-testing and operational modal analysis of the Humber Bridge. *Engineering Structures, 32*(8), 2003–2018. https://doi.org/10.1016/j.engstruct.2010.02.034

Brownjohn, J. M., Koo, K.-Y., Scullion, A., & List, D. (2020). Operational deformations in long-span bridges. In Design, assessment, monitoring

and maintenance of bridges and infrastructure networks (pp. 144–162). Routledge. https://doi.org/10.1201/9781351038140-10

Chen, J., Chajes, M. J., & Shenton, H. W. (2023). Impact of wind load characteristics on computed bridge stay-cable forces used for bridge health monitoring. *Journal of Bridge Engineering, 28*(4), Article 04023007. https://doi.org/doi:10.1061/JBENF2.BEENG-5832

Cheynet, E., Daniotti, N., Jakobsen, J. B., & Snæbjörnsson, J. (2020). Improved long-span bridge modeling using data-driven identification of vehicle-induced vibrations. *Structural Control and Health Monitoring, 27*(9), Article e2574. https://doi.org/10.1002/stc.2574

Dederichs, A. C., & Øiseth, O. (2023). Experimental comparison of automatic operational modal analysis algorithms for application to long-span road bridges. *Mechanical Systems and Signal Processing, 199*, Article 110485. https://doi.org/10.1016/j.ymssp.2023.110485

Freimanis, A., & Paeglitis, A. (2020). Crack development assessment using modal analysis in peridynamic theory. *Journal of Computational Design and Engineering, 8*(1), 125–139. https://doi.org/10.1093/jcde/qwaa066

Freimanis, A., & Paeglītis, A. (2019). Modal analysis of healthy and cracked isotropic plates in peridynamics. In M. Mains & B. J. Dilworth (eds.), *Topics in Modal Analysis & Testing*, *9*, Springer, Cham. https://doi.org/10.1007/978-3-319-74700-2_41

Gatti, M. (2019). Structural health monitoring of an operational bridge: A case study. *Engineering Structures, 195*, 200–209. https://doi.org/10.1016/j.engstruct.2019.05.102

Górski, P., Napieraj, M., & Konopka, E. (2020). Variability evaluation of dynamic characteristics of highway steel bridge based on daily traffic-induced vibrations. *Measurement, 164*, Article 108074. https://doi.org/10.1016/j.measurement.2020.108074

Gundewar, S. K., & Kane, P. V. (2022). Bearing fault diagnosis using time segmented Fourier synchrosqueezed transform images and convolution neural network. *Measurement, 203*, Article 111855. https://doi.org/10.1016/j.measurement.2022.111855

Ha, T.-H., Chou, T.-Y., & Fang, Y.-M. (2020). Assessment of bridge deck movement under the impact of environmental factors and traffic load. *IOP Conference Series: Materials Science and Engineering*, *884*, Article 012038 https://doi.org/10.1088/1757-899X/884/1/012038

He, Z., Li, W., Salehi, H., Zhang, H., Zhou, H., & Jiao, P. (2022). Integrated structural health monitoring in bridge engineering. *Automation in Construction, 136*, Article 104168. https://doi.org/10.1016/j.autcon.2022.104168

Ho, H., & Nishio, M. (2020). Evaluation of dynamic responses of bridges considering traffic flow and surface roughness. *Engineering Structures, 225*, Article 111256. https://doi.org/10.1016/j.engstruct.2020.111256

Huang, H.-B., Yi, T.-H., Li, H.-N., & Liu, H. (2020). Strain-based performance warning method for bridge main girders under variable operating conditions. *Journal of Bridge Engineering, 25*(4), Article 04020013. https://doi.org/10.1061/(ASCE)BE.1943-5592.0001538

Kareem, A., & Kijewski, T. (2002). Time-frequency analysis of wind effects on structures. *Journal of Wind Engineering and Industrial Aerodynamics, 90*(12–15), 1435–1452. https://doi.org/https://doi.org/10.1016/S0167-6105(02)00263-5

Ko, J., & Ni, Y. Q. (2005). Technology developments in structural health monitoring of large-scale bridges. *Engineering Structures, 27*(12), 1715–1725. https://doi.org/10.1016/j.engstruct.2005.02.021

Koo, K.-Y., Brownjohn, J., List, D., & Cole, R. (2013). Structural health monitoring of the Tamar suspension bridge. *Structural Control and Health Monitoring, 20*(4), 609–625. https://doi.org/10.1002/stc.1481

Lu, L., & Ren, W.-X. (2023). Structural instantaneous frequency identification based on synchrosqueezing fractional Fourier transform. Structures, *56*, Article 104914. https://doi.org/10.1016/j.istruc.2023.104914

Lu, N., Ma, Y., & Liu, Y. (2019). Evaluating probabilistic traffic load effects on large bridges using long-term traffic monitoring data. *Sensors, 19*(22), Article 5056. https://doi.org/10.3390/s19225056

Magalhães, F., Cunha, Á., & Caetano, E. (2012). Vibration based structural health monitoring of an arch bridge: From automated OMA to damage detection. *Mechanical Systems and Signal Processing, 28*, 212–228. https://doi.org/10.1016/j.ymssp.2011.06.011

Maljaars, J. (2020). Evaluation of traffic load models for fatigue verification of European road bridges. *Engineering Structures, 225*, Article 111326. https://doi.org/10.1016/j.engstruct.2020.111326

Mariani, S., Kalantari, A., Kromanis, R., & Marzani, A. (2024). Data-driven modeling of long temperature time-series to capture the thermal behavior of bridges for SHM purposes. *Mechanical Systems and Signal Processing, 206*, Article 110934. https://doi.org/10.1016/j.ymssp.2023.110934

Mostafa, N., Di Maio, D., Loendersloot, R., & Tinga, T. (2021). Extracting the time-dependent resonances of a vehicle–bridge interacting system by wavelet synchrosqueezed transform. *Structural Control and Health Monitoring, 28*(12), Article e2833. https://doi.org/10.1002/stc.2833

Neild, S. A., McFadden, P. D., & Williams, M. S. (2003). A review of time-frequency methods for structural vibration analysis. *Engineering Structures, 25*(6), 713–728. https://doi.org/https://doi.org/10.1016/S0141-0296(02)00194-3

Nicoletti, V., Quarchioni, S., Tentella, L., Martini, R., & Gara, F. (2023). Experimental tests and numerical analyses for the dynamic characterization of a steel and wooden cable-stayed footbridge. *Infrastructures, 8*(6), Article 100. https://doi.org/10.3390/infrastructures8060100

Oberlin, T., Meignen, S., & Perrier, V. (2014). The Fourier-based synchrosqueezing transform. 2014 IEEE International Conference on Acoustics, Speech and Signal Processing (ICASSP), Florence, Italy, 315–319. https://doi.org/10.1109/ICASSP.2014.6853609

Omenzetter, P., Beskhyroun, S., Shabbir, F., Chen, G.-W., Chen, X., Wang, S., & Zha, A. (2013). *Forced and ambient vibration testing of full scale bridges* (Report number: UNI/578). Earthquake Commission Research Foundation. https://doi.org/10.13140/2.1.1168.5448

Prat, M. (2001). Traffic load models for bridge design: recent developments and research. *Progress in Structural Engineering and Materials, 3*(4), 326-334.

Qin, Y. (2023). Investigating bridge vibrational modes under operational conditions using time-frequency analysis. *Structure and Infrastructure Engineering*, 1–15. https://doi.org/10.1080/15732479.2023.2275684

Silik, A., Noori, M., Altabey, W. A., Ghiasi, R., & Wu, Z. (2021). Comparative analysis of wavelet transform for time-frequency analysis and transient localization in structural health monitoring. *Structural Durability & Health Monitoring, 15*(1), 1–22. https://doi.org/10.32604/sdhm.2021.012751

Solomon, O. M. (1991). *PSD computations using Welch's method* (Sandia Report SAND 91-1533, UC-706). Sandia National Laboratories. https://www.osti.gov/servlets/purl/5688766

Stoica, P., & Moses, R. L. (2005). *Spectral analysis of signals* (Vol. 452). Pearson Prentice Hall Upper Saddle River, NJ.

Tang, L., Shang, X.-Q., Huang, T.-L., Wang, N.-B., & Ren, W.-X. (2023). An improved local maximum synchrosqueezing transform with adaptive window width for instantaneous frequency identification of time-varying structures. *Engineering Structures, 292*, Article 116543. https://doi.org/10.1016/j.engstruct.2023.116543

Tran, N. H., Khatir, S., De Roeck, G., Nguyen, L., Bui, T. T., & Abdel Wahab, M. (2020). An efficient approach for model updating of a large-scale cable-stayed bridge using ambient vibration measurements combined with a hybrid metaheuristic search algorithm. *Smart Structures and Systems, 25*(4), 487–499.

Villwock, S., & Pacas, M. (2008). Application of the Welch-method for the identification of two-and three-mass-systems. *IEEE Transactions on Industrial Electronics, 55*(1), 457–466. https://doi.org/10.1109/TIE.2007.909753

Wattana, K., & Nishio, M. (2017). Application of a regression model for predicting traffic volume from dynamic monitoring data to the bridge safety evaluation. *Journal of Civil Structural Health Monitoring, 7*, 429–443. https://doi.org/10.1007/s13349-017-0234-7

Westgate, R., Koo, K.-Y., & Brownjohn, J. (2015). Effect of vehicular loading on suspension bridge dynamic properties. *Structure and Infrastructure Engineering, 11*(2), 129–144. https://doi.org/10.1080/15732479.2013.850731

Xu, X., Xu, Y.-L., Ren, Y., & Huang, Q. (2021). Site-specific extreme load estimation of a long-span cable-stayed bridge. *Journal of Bridge Engineering, 26*(4), Article 05021001. https://doi.org/doi:10.1061/(ASCE)BE.1943-5592.0001700

Yang, Y. B., Yang, M., Liu, D.-H., Liu, Y. H., & Xu, H. (2024). Bridge damping formula based on instantaneous amplitudes of vehicle's front and rear contact responses by Hilbert transform. *International Journal of Structural Stability and Dynamics, 24*(15), Article 2471006. https://doi.org/10.1142/s0219455424710068

Ye, X., Wu, P., Liu, A., Zhan, X., Wang, Z., & Zhao, Y. (2023). A deep learning-based method for automatic abnormal data detection: Case study for bridge

structural health monitoring. *International Journal of Structural Stability and Dynamics*, *23*(11), Article 2350131.
https://doi.org/10.1142/S0219455423501316

Zahid, F. B., Ong, Z. C., & Khoo, S. Y. (2020). A review of operational modal analysis techniques for in-service modal identification. *Journal of the Brazilian Society of Mechanical Sciences and Engineering, 42*, 1–18.
https://doi.org/10.1007/s40430-020-02470-8

Zhang, G.-Q., Xu, Y.-L., Dan, D.-H., Jiang, S.-J., & Zhu, Q. (2024). Simulation and prediction of vortex-induced vibration of a long suspension bridge using SHM-based digital twin technology. *Journal of Wind Engineering and Industrial Aerodynamics, 247*, Article 105705.
https://doi.org/10.1016/j.jweia.2024.105705

Zhang, Q., Fan, L., & Yuan, W. (2002). Traffic-induced variability in dynamic properties of cable-stayed bridge. *Earthquake Engineering & Structural Dynamics, 31*(11), 2015–2021. https://doi.org/10.1002/eqe.204

Zhang, X., Lu, Y., Cao, M., Li, S., Sumarac, D., & Wang, Z. (2022). Instantaneous identification of tension in bridge cables using synchrosqueezing wave-packet transform of acceleration responses. *Structure and Infrastructure Engineering*, 20(2), 199–214.
https://doi.org/10.1080/15732479.2022.2082492

Zheng, J., Tang, J., Zhou, Z., Heng, J., Chu, X., & Wu, T. (2022). Intelligent cognition of traffic loads on road bridges: From measurement to simulation – A review. *Measurement*, *200*, Article 111636.
https://doi.org/10.1016/j.measurement.2022.111636

Zhou, J., Caprani, C. C., & Zhang, L. (2021). On the structural safety of long-span bridges under traffic loadings caused by maintenance works. *Engineering Structures, 240*, Article 112407.
https://doi.org/10.1016/j.engstruct.2021.112407

Zhou, Y., & Sun, L. (2019). Effects of environmental and operational actions on the modal frequency variations of a sea-crossing bridge: A periodicity perspective. *Mechanical Systems and Signal Processing, 131*, 505–523.
https://doi.org/https://doi.org/10.1016/j.ymssp.2019.05.063